Multiple self-localized electronic states in *trans*-polyacetylene

Xi Lin*, Ju Li‡, Clemens J. Först*, and Sidney Yip*§

*Departments of Nuclear Science and Engineering and Materials Science and Engineering, Massachusetts Institute of Technology, Cambridge, MA 02139; and ‡Department of Materials Science and Engineering, Ohio State University, Columbus, OH 43210

Edited by Esther M. Conwell, University of Rochester, Rochester, NY, and approved April 26, 2006 (received for review February 15, 2006)

Electronic structure calculations on a conjugated polymer chain by Hartree–Fock and density functional theory show a sequence of self-localized states, which stand in contrast to the single self-localized soliton state described by the Su–Schrieffer–Heeger model Hamiltonian. An extended Hubbard model, which treats electron–electron interactions up to second neighbors, is constructed to demonstrate that the additional states arise from a strong band-bending effect due to the presence of localized electric fields of charged solitons. We suggest the optical response of these electronic states may be associated with the near-edge oscillations observed in photo-induced absorption spectra. Our calculations indicate further that in the presence of counterions, the additional localized states continue to exist. Implications regarding soliton mobility and high-resolution ion sensing are briefly discussed.

conducting polymer | self-localization | soliton

Conjugated polymers exhibit remarkable electronic, optical, magnetic, and actuation properties (1–4), which make them attractive for device applications. Theoretical understanding of these fourth-generation polymeric materials (5) lies in the concept of self-localized solitons, originally proposed by Su, Shrieffer, and Heeger (SSH) in their model Hamiltonian (6, 7) for *trans*-polyacetylene (*t*-PA). A few distinct characteristics of the soliton are illustrated in Fig. 1. One sees an order parameter profile in the form of a domain wall (Fig. 1*a*), a density of states (DOS) plot with a single state located in the middle of the gap (Fig. 1*b*), and localized vs. delocalized wavefunctions, respectively, for the soliton and band states (Fig. 1*c*). Experiments have confirmed the existence of the midgap state of the SSH model (7); additionally, effects of neglected electron correlations (8–13) and counterion potentials (14, 15) on many properties of photo-excited and chemically doped polymers have been investigated. In particular, Hubbard models and first-principles computations have elucidated important characteristic properties of conjugated polymers, such as enhancement of Peierls distortion (10, 11), negative spin density waves (12, 13), fundamental band gap (16, 17), polaron and bipolaron formation (18), polaron-coupled polymer secondary structures (19), and polaron interchain transport (20, 21). However, few discussions have been given to the effects of electron correlation and counterion on extended π bands, except for the study by Strafstrom and Chao (22) showing that the local DOS of the SSH soliton depletes the local DOS of π bands at the same sites. In this work, we show that electron correlations lead to additional, previously undescribed localization effects, regardless of the absence or presence of counterions, in a study of the *t*-PA system by using first-principles Hartree–Fock (HF) and density functional theory (DFT) methods. Fig. 2 shows the DOS for the σ and π electrons obtained by HF/3-21G and DFT hybrid BHandHLYP/3-21G (23), for the positive-charge soliton S^+. In contrast to the single gap state in Fig. 1, several states appear in Fig. 2. To our knowledge, a demonstration of multiple self-localized states in conjugated polymers has not been described previously. To investigate the nature of these additional states in the gap, we analyze an extended Hubbard model as extension of the SSH Hamiltonian to include electron–electron interactions. The additional localized states are found to arise from local shifts in the valence and conduction bands induced by the presence of charged solitons, similar to the band-bending mechanism well known from semiconductor heterojunctions. Such localizations persist in the presence of counterions.

We consider the extended Hubbard Hamiltonian

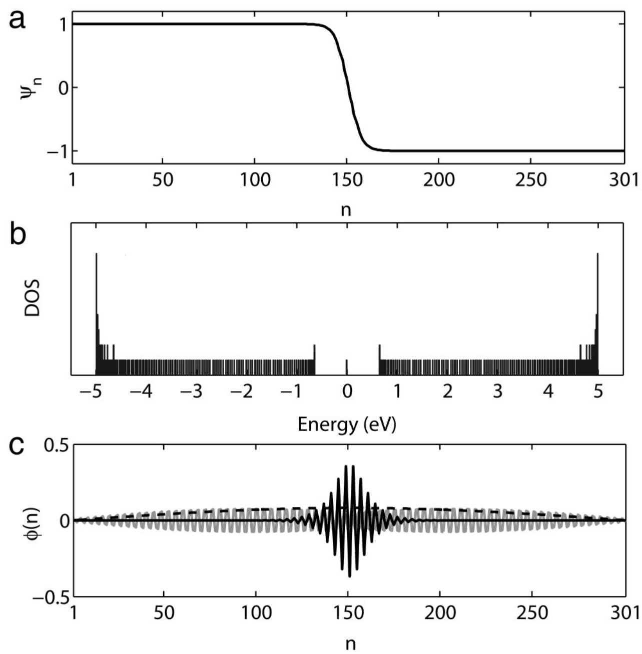

Fig. 1. Properties of the soliton described by the SSH Hamiltonian (Eq. **2**) for a 301-unit *t*-PA: order parameter profile $\psi_n = (-1)^n u_n$ showing the domain wall (*a*), DOS showing the single gap state (*b*), and eigenfunctions $\phi(n)$ showing the spatial self-localization of the soliton (*c*), where *n* labels the CH unit sites. Original parameter values are used as follows: $K = 21$ eV/Å^2, $t_0 = 2.5$ eV, and $\alpha = 4.1$ eV/Å (6). The soliton state $\phi_s(n)$ (solid black) is exponentially localized, in contrast to delocalized valence and conduction band states (only the lowest valence and conduction states are shown in dashed and gray lines respectively). Solitons may exist in three electronic states: neutral and singly occupied (S^0), positively charged and unoccupied (S^+), and negatively charged and doubly occupied (S^-).

Conflict of interest statement: No conflicts declared.

This paper was submitted directly (Track II) to the PNAS office.

Abbreviations: CH, carbon–hydrogen; DFT, density functional theory; DOS, density of states; HF, Hartree–Fock; SSH, Su, Shrieffer, and Heeger; *t*-PA, *trans*-polyacetylene.

§To whom correspondence should be addressed. E-mail: syip@mit.edu.

PHYSICS

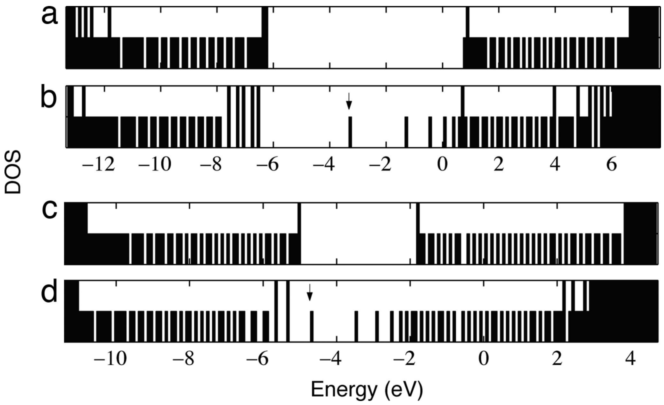

Fig. 2. DOS of both σ and π electrons calculated by HF/3-21G (23) for a 160-unit defect-free *t*-PA (*a*) and 161-unit *t*-PA with S^+ (*b*), and by the hybrid DFT BHandHLYP/3-21G method (23) for a 160-unit defect-free *t*-PA (*c*) and 161-unit with S^+ (*d*). The SSH soliton states are marked by an arrow.

$$H = H_{\mathrm{SSH}} + \sum_{i=0}^{2} H_{0i}^{ee},$$

$$H_{00}^{ee} = \frac{U}{2} \sum_{n,\sigma} (c_{n,\sigma}^{\dagger} c_{n,\sigma} c_{n,-\sigma}^{\dagger} c_{n,-\sigma}), \qquad [1]$$

$$H_{0i}^{ee} = \sum_{n} V_{0i}\left(-1 + \sum_{\sigma} c_{n,\sigma}^{\dagger} c_{n,\sigma}\right)\left(-1 + \sum_{\sigma'} c_{n+i,\sigma'}^{\dagger} c_{n+i,\sigma'}\right), \quad i = 1, 2,$$

where the SSH Hamiltonian is

$$H_{\mathrm{SSH}} = \sum_{n} \frac{p_n^2}{2\mu} + \sum_{n} \frac{1}{2} K_n (u_{n+1} - u_n)^2 + \sum_{n,\sigma} [-t_0 + \alpha(u_{n+1} - u_n)] \cdot (c_{n+1,\sigma}^{\dagger} c_{n,\sigma} + c_{n,\sigma}^{\dagger} c_{n+1,\sigma}). \qquad [2]$$

In Eqs. **1** and **2**, U and V are the on- and off-site Coulomb repulsion strengths, respectively; p is the atomic momentum; μ is the mass of a carbon–hydrogen (CH) unit; K is the spring constant representing the σ bonding between adjacent CH units; u is the atomic displacement with respect to the undimerized chain; t_0 is the hopping integral of the undimerized chain; α is the linear electron–phonon coupling constant; and $c_{n,\sigma}^{\dagger}$ and $c_{n,\sigma}$ are creation and annihilation operators for π-electron of spin σ at site n, respectively. In view of the importance of Coulomb charge interactions as explained in detail below, we choose to solve the extended Hubbard model (1) under the unrestricted HF approximation (12).

By switching on U and V interactions, we find that both the valence and conduction bands respond strongly to the localized charge distributions in solitons with positive and negative charges, S^+ and S^-. Although this process leads to eigenstate hybridization in the Hilbert space of π electrons, little hybridization occurs between the valence and conduction subspaces across the $\approx$1.5-eV band gap (1 eV = 1.602×10^{-19} J). In the case of S^+ where the localized net charge distribution is positive, the Hamiltonian (1) creates a locally attractive potential acting on the electrons of the neighboring CH sites. This change causes the energies of the bottom valence and conduction band states to move into the forbidden regions, thereby forming new interfacial misfit states, whose wavefunctions tunnel into the +1 and −1 phases with characteristic exponentially decaying tails as described by the complex band structure theory (24, 25). The effect is similar to the band-bending phenomena known to occur at semiconductor heterojunctions and surfaces (26), except that here the much shorter localization length scale is caused by the primary self-trapping soliton state carrying a single elementary charge. The overall band bending computed by using standard tight-binding parameters from the literature (6, 12, 27) is shown in an energy-site plot, Fig. 3, that combines energy information with spatial distribution of the wavefunction (juxtaposed local DOS plots). Five localized gap states are seen to stand out (labeled *a*–*e* and further displayed in Fig. 4). Their wavefunctions are in sharp contrast to the reconstructed delocalized valence and conduction band states, which also are shown in Fig. 3.

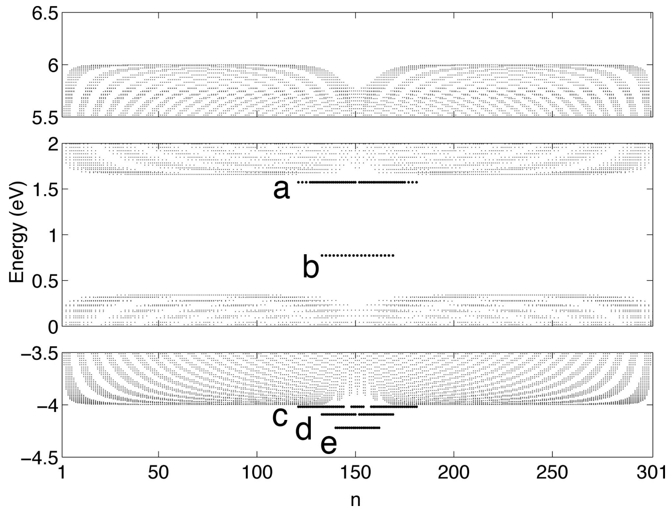

Fig. 3. Energy-site plot of the eigenfunctions of the extended Hubbard model (Eq. **1**) for a 301-unit *t*-PA with S^+. For every eigenstate, individual site n is marked by a dot if and only if the eigenfunction component on that site is $\geq$1/301. The blank regions between two adjacent dots reflect the corresponding nodal structure of an eigenfunction, where the lowest state (*e*) has no node, the next lowest state (*d*) has one node, *c* has two, *b* has 150, and *a* has 151 nodes (see Fig. 4 for the spatial distribution of these five states). In addition to the original SSH parameters (6), the following standard parameters are used: U = 4.0 eV (12), V_{01} = $(U/2)\cdot(7.55/11.0)$ (27), and V_{02} = $(U/2)\cdot(5.2/11.0)$ (27).

The behavior of S^- is completely symmetric to S^+ in that a repulsive potential is created, which leads to the depletion of band states at the bottom of valence and conduction bands in the interfacial region, resulting in the creation of localized states at the top of both bands. Similar self-localized states are thus obtained but with valence and conduction bands bending upwards.

Through parametric studies we find the behavior just described to persist over a wide range of U and V values. For a reasonable set of parameters, U = 4.0 eV (12), V_{01} = $(U/2)\cdot(7.55/11.0)$ (27), and V_{02} = $(U/2)\cdot(5.2/11.0)$ (27); the primary gap state (Fig. 3*b*) appears at 0.23 eV below the gap center, which would correspond to the 0.5-eV peak [the so-called low-energy (LE) band that was 0.25 eV below the gap center] observed in photo-induced absorption (PA) experiments; it was assigned to charged solitons $S^{\pm}$ (28). Another excitation would appear at 1.30 eV (Fig. 3*a*) from the valence band edge, overlapping in energy with two distinct experimental PA features. One feature is the so-called high-energy (HE) band, which has been assigned to neutral solitons S^0 because of different responses to magnetic excitation (29, 30), temperature (9), optical polarization (31),

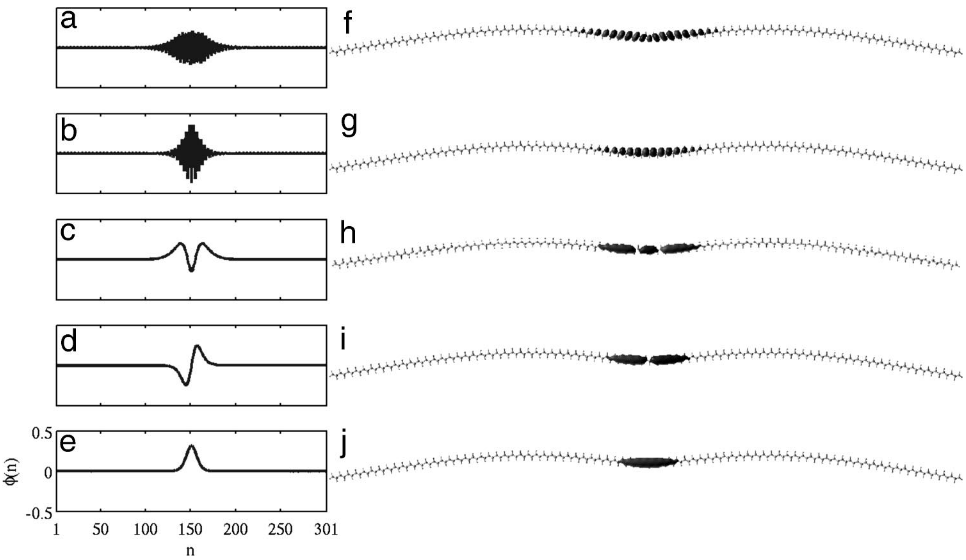

Fig. 4. Comparison of the five localized S^+ electronic states (*a–e*) of a 301-unit *t*-PA described by the extended Hubbard model with the corresponding results (*f–j*) obtained by HF/3-21G calculation for a 161-unit *t*-PA. States *a–e* are the same as those shown in Fig. 3. In *f–j*, red and blue lobes, wavefunction contour isosurface value of ± 0.01 Å$^{-3/2}$, denote different phases so that *j* has no node, *i* has 1 node, *h* has 2, *g* has 80, and *f* has 81 nodes.

and disorder of the sample (31) from the LE band. Another feature is the near-edge oscillatory structure observed in the PA spectra (8), believed to be due to strong electric field polarization of the surrounding medium caused by charged solitons (electro-absorption effect at the microscopic length scale). This explanation has the same physical origin as our secondary localized states.

To verify the predictions of the extended Hubbard model (Eq. **2**), we return to the original HF and DFT results. We find that in the case of S^+, additional localized π states are deeply buried in the σ bands, below the valence π band, which were not shown in the DOS plot (Fig. 2). These low-lying localized states are in agreement with the extended-Hubbard predictions (Fig. 4). Moreover, full geometry optimizations in both HF and DFT computations lead to a strong $S^{\pm}$ soliton-induced carbon backbone bending. It is important to note that this result is not a straightforward consequence of electrostatic repulsion among the charged CH sites (4).

We have thus far demonstrated that the secondary localized electronic states are intrinsically induced by photo-generated solitons (28, 32). Now we consider how counterions, carrying opposite charges to the SSH solitons, affect the localizations in chemically doped polymers. We have performed HF and DFT calculations explicitly treating several counterions species anions, F^-, Cl^-, ClO_4^-, PF_6^-, and $N(SO_2CF_3)_2^-$, and cations, Li^+ and Na^+. We find in all these cases at least one additional secondary localized state stands out from the valence and conduction bands (Fig. 5). Fig. 5 shows two characteristic properties of the secondary localized states in the case of Cl^- counterion, their energies being located in the forbidden regions and their wavefunctions containing exponentially decaying wave tails. Detailed comparisons with the SSH soliton wavefunction indicate that the lowest additional localized state below the valence band S_v is as localized as the SSH soliton state, whereas the lowest additional localized state below the conduction band S_c is less localized. We also have investigated solvent screening effects by using the Polarizable Continuum Model (23), and no discernable effects on either the energy or wavefunction localization were found. It may be useful to emphasize that the secondary localized states discussed in the present work are an intrinsic manifestation of electron correlation effects on extended π bands, distinct from extrinsic effects such as counterions and solvent molecules, which may affect many important physical properties of conjugated polymers (14, 15).

The present results have several implications. First, the appearance of multiple localized states centered on the same site of the polymer chain creates additional lattice distortions, which may have nonnegligible effects on soliton mobility. With the soliton having to drag along the localized band reorganizations, lattice distortions, and chain conformation changes, its effective mass may be significantly different from the $6m_e$ estimated in the original SSH model (33). Second, besides the states in the π-band gap, self-localized states also exist below the valence π

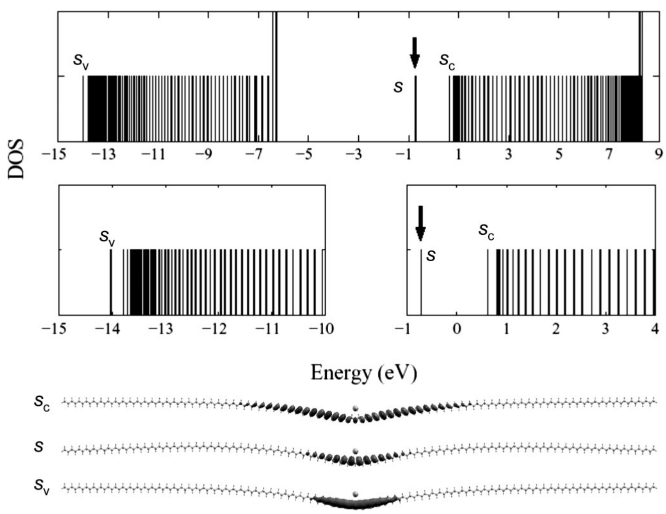

Fig. 5. DOS of the complete π eigenstates (*Upper*) and two close-up views of the bottom valence and conduction π band (*Lower*), respectively, calculated by HF/3-21G (23) for a 161-unit *t*-PA doped by a chlorine counterion. Three exponentially localized wavefunctions are plotted with contour isosurface value of ± 0.01 Å$^{-3/2}$, namely, the lowest additional localized state below the conduction band S_c, the SSH soliton state S (marked by an arrow), and the lowest additional localized state below the valence band S_v. The Cl^- anion, large sphere close the chain center, is 3.4 Å from the closest C atom on the *t*-PA chain.

band (S^+) and above the conduction π band (S^-). As shown in Fig. 2, discrete states below the valence π band are buried in the continuum σ band and therefore cannot be seen in terms of excitation energy only. However, in view of the selection rules based on orbital symmetry for transitions among π states, these intrinsic excitations should be detectable by photo-scattering measurements on highly stretch-aligned films (34) or layer-by-layer-assembled films (35). In this connection we estimate the excitation energy from the lowest localized state (Fig. 3*e*) to the conduction band edge to be 6.1 eV. Lastly, as can be seen in Figs. 2*b* and 5, the presence of counterions causes the energy of secondary localized states to shift toward the corresponding band edge, which demonstrates the sensitivity of these states to external fields. For example, our calculations find the width of the primary localized state does not change appreciably in the presence of F^- or PF_6^- counterions, but the width of the secondary localized state of the former is 30% wider than the latter. This sensitivity to the presence of local external electric fields may provide opportunities for ion sensing.

This work was supported by Honda R&D Co., Ltd.; the Defense Advanced Research Planning Agency/Office of Naval Research; Office of Naval Research Grant N00014-05-1-0504; Air Force Office of Scientific Research Grant FA9550-05-1-0026; National Science Foundation Grants ITR-020541, DMR-0325553, and IMR-0414849; the National Energy Technology Laboratory; the Lawrence Livermore National Laboratory; and the Ohio Supercomputer Center.

1. Burroughes, J. H., Jones, C. A. & Friend, R. H. (1988) *Nature* **335,** 137–141.
2. Yu, Y., Nakano, M. & Ikeda, T. (2003) *Nature* **425,** 145.
3. Kubatkin, S., Danilov, A., Hjort, M., Cornil, J., Bredas, J.-L., Stuhr-Hansen, N., Hedegard, P. & Bjorholm, T. (2003) *Nature* **425,** 698–701.
4. Lin, X., Li, J. & Yip, S. (2005) *Phys. Rev. Lett.* **95,** 198303.
5. Heeger, A. J. (2001) *Rev. Mod. Phys.* **73,** 681–700.
6. Su, W. P., Schrieffer, J. R. & Heeger, A. J. (1979) *Phys. Rev. Lett.* **42,** 1698–1701.
7. Heeger, A. J., Kivelson, S., Schrieffer, J. R. & Su, W.-P. (1988) *Rev. Mod. Phys.* **60,** 781–851.
8. Orenstein, J. (1986) in *Handbook of Conducting Polymers*, ed. Skotheim, T. A. (Dekker, New York), Vol. 2, pp. 1297–1335.
9. Vardeny, Z. V. & Wei, X. (1998) in *Handbook of Conducting Polymers*, eds. Skotheim, T. A., Elsenbaumer, R. L. & Reynolds, J. R. (Dekker, New York), pp. 639–666.
10. Hirsch, J. E. (1983) *Phys. Rev. Lett.* **51,** 296–299.
11. Hayden, G. W. & Mele, E. J. (1985) *Phys. Rev. B Condens. Matter* **32,** 6527–6530.
12. Subbaswamy, K. R. & Grabowski, M. (1981) *Phys. Rev. B Condens. Matter* **24,** 2168–2173.
13. Soos, Z. G. & Ramasesha, S. (1983) *Phys. Rev. Lett.* **51,** 2374–2377.
14. Colle, R. & Curioni, A. (1998) *J. Am. Chem. Soc.* **120,** 4832–4839.
15. Brédas, J. L., Thémans, B., Fripiat, J. G., André, J. M. & Chance, R. R. (1984) *Phys. Rev. B Condens. Matter* **29,** 6761–6773.
16. Brédas, J. L. (1985) *J. Chem. Phys.* **82,** 3808–3811.
17. Ma, J., Li, S. & Jiang, Y. (2002) *Macromolecules* **35,** 1109–1115.
18. Brédas, J. L., Scott, J. C., Yakushi, K. & Street, G. B. (1984) *Phys. Rev. B Condens. Matter* **30,** 1023–1025.
19. Lin, X., Li, J., Smela, E. & Yip, S. (2005) *Int. J. Quant. Chem.* **102,** 980–985.
20. Brédas, J. L., Calbert, J. P., da Silva Filho, D. A. & Cornil, J. (2002) *Proc. Natl. Acad. Sci. USA* **99,** 5804–5809.
21. Ferretti, A., Ruini, A., Molinari, E. & Caldas, M. (2003) *Phys. Rev. Lett.* **90,** 086401.
22. Strafstrom, S. & Chao, K. A. (1984) *Phys. Rev. B Condens. Matter* **29,** 2255–2266.
23. Frisch, M. J., Trucks, G. W., Schlegel, H. B., Scuseria, G. E., Robb, M. A., Cheeseman, J. R., Montgomery, J. A., Vreven, T., Kudin, K. N. & Burant, J. C., *et al*. (2003) GAUSSIAN 03 (Gaussian, Pittsburgh), Revision C.02.
24. Kohn, W. (1959) *Phys. Rev.* **115,** 809–821.
25. Tomfohr, J. K. & Sankey, O. F. (2002) *Phys. Rev. B Condens. Matter* **65,** 245105.
26. Marder, M. P. (2000) *Condensed Matter Physics* (Wiley, New York).
27. Dewar, M. J. (1969) *The Molecular Orbital Theory of Organic Chemistry* (McGraw–Hill, New York).
28. Orenstein, J. & Baker, G. L. (1982) *Phys. Rev. Lett.* **49,** 1043–1046.
29. Wei, X., Hess, B. C., Vardeny, Z. V. & Wudl, F. (1992) *Phys. Rev. Lett.* **68,** 666.
30. Vardeny, Z. V. & Wei, X. (1993) *Synthetic Metals* **54,** 99–111.
31. Friend, R. H., Bradley, D. D. C. & Townsend, P. D. (1987) *J. Phys. D Appl. Phys.* **20,** 1367–1384.
32. Su, W. P. & Schrieffer, J. R. (1980) *Proc. Natl. Acad. Sci. USA* **77,** 5626–5629.
33. Su, W. P., Schrieffer, J. R. & Heeger, A. J. (1980) *Phys. Rev. B Condens. Matter* **22,** 2099–2110.
34. Shirakawa, H. & Ikeda, S. (1980) *Synthetic Metals* **1,** 175–184.
35. Ho, P. K. H., Kim, J.-S., Burroughes, J. H., Becker, H., Li, S. F. Y., Brown, T. M., Cacialli, F. & Friend, R. H. (2000) *Nature* **404,** 481–484.